Invited Paper

Silicon micro-optics for smart light control

G. Vdovin, D.W. de Lima Monteiro, O. Akhzar-Mehr, M. Loktev,
S. Sakarya, O. Soloviev and P.M. Sarro

Electronic Instrumentation, ITS, Delft University of Technology,
Mekelweg 4, 2628 CD, Delft, The Netherlands

ABSTRACT

We present an overview of the results of our recent research in the field of adaptive optical components based on silicon microtechnologies, including membrane deformable mirrors, spatial light modulators, liquid-crystal correctors, wavefront sensors, and both spherical and aspherical micro-optical components. We aim at the realization of adaptive optical systems using standard-technology solutions.

Keywords: adaptive optics, deformable mirror, wavefront sensor, liquid-crystal corrector, spatial light modulator, microlens arrays, aspherics, micromachining, CMOS

1. INTRODUCTION

Adaptive optics has a strong potential for applications in industry and medicine, but its effective usability in these fields requires further development of wavefront sensors and correctors. Some of the desired characteristics are that they can be fabricated in a process as standard as possible, that they are easily scalable and reproducible, that they offer flexibility of design and, especially, that they are compatible with restricted budgets.

Silicon technology is widely available and encompasses mature microelectronic and micromachining processes, which guarantee reasonable processing costs, design flexibility and good yield. We use the features of these standard processes in the mechanical and electronic domains to fabricate high-quality and inexpensive optical devices for adaptive optical systems.

In the present overview we report on our recent results in micromachined adaptive optics, CMOS wavefront sensors, liquid crystal adaptive optics with modal response and bulk micromachined spherical and aspherical surfaces.

2. VISCOELASTIC SPATIAL LIGHT MODULATORS (SLM)

In recent years , there has been an increasing commercial interest and investment into the field of miniature optical components that are fabricated on a microscale for a wide variety of purposes ranging from optical elements in mobile devices,[1] projection displays and optical communication networks. Since each field by itself comprises billion dollar markets,[2] the combined potential justifies academic exploration into approaches toward uniform technology applicable within a large context.

In order to allow for mass deployment beyond just several specialized custom-designed applications, a number of stringent requirements need to be met in the areas of reproducibility, quality, performance and especially low per-unit fabrication and maintenance costs.[3]

Historically, there has already been interest since the past decades in using silicon as a mechanical material for both sensors and actuators[4] and during the past decade an increasingly widespread interest is seen in micromechanical systems, followed by similarly increasing allocation of research budgets to these diverse fields.[5]

Further author information: G. Vdovin: email: gleb@titus.et.tudelft.nl, tel/fax:+31-15-278-6165/5755; D.W. de Lima Monteiro: email: davies@titus.et.tudelft.nl, tel: +31-15-2786285

MOEMS Display and Imaging Systems II, edited by Hakan Urey, David L. Dickensheets,
Proceedings of SPIE Vol. 5348 (SPIE, Bellingham, WA, 2004)
0277-786X/04/$15 · doi: 10.1117/12.532482

2.1. Principle of operation

There are three main areas of application for viscoelastic SLM:

- Projection displays, in particular solid-state alternatives for Eidophor projectors.
- Optical components for information processing systems and communication networks.
- Adaptive optics with very large number of control channels.

The modulation principle explored in the previous research involves a sinusoidal phase grating implemented on a viscoelastic support layer. This grating is achieved by placing alternating potentials on an underlying electrode structure, which results in electrostatic forces pulling in the affected regions, as shown in Fig. 1.

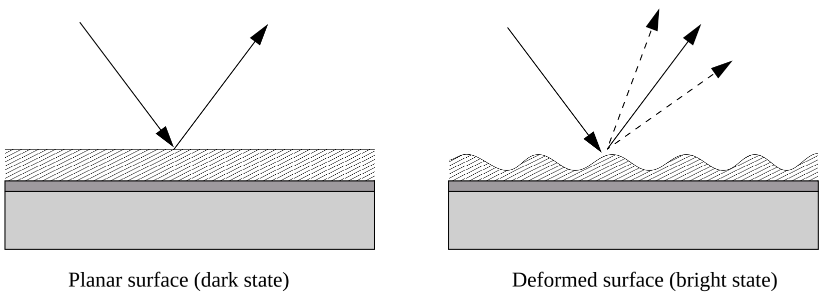

Figure 1. Side-view schematic for no potentials applied (left) and alternating potentials applied (right).

The motivation behind the viscoelastic layer approach was to find a solid-state alternative to Eidophor projectors. These provide high light output of up to 10000lm at contrast ratios in the order of 300:1. However, these are complex to manufacture and carry high maintenance costs, thus inhibiting mass deployment.[6,7]

Single-pixel VSLM demonstrators have been fabricated in the lab with a thickness of 5-35μm over a periodic aluminum electrode structure. The top surface consists of a metal layer (80nm of Al or Au) and an optional protective layer (50nm of SiN).

The reflecting surface has a 100% fill factor in the sense that all light is reflected over the entire area since there are no mandatory intermediate gaps between the pixels. In addition to a flexibility in choice of coatings, this allows the technology to be optimized within a wide spectral range, including IR and UV at high levels of incident optical power.

2.1.1. Modulation principle for projectors

To use fully reflective phase modulators, an optical setup is required to map variations in phase to variations in intensity. An example of such a setup for a single pixel is shown in Fig. 2. The incoming light is reflected from the Schlieren bars into the Schlieren lens. If the pixel is planar, the light is reflected back onto the stops. If the pixel is sinusoidally deformed, different beam paths will result, some of which will pass the stops and enter the projection lens. This lens images the pixel to a corresponding position on the projection screen.

The efficiency of the system is described in the ability of moving optical power out of the zero order (corresponding to planar) state into the other orders. The relative efficiency for each order n can be calculated from Bessel functions:

$$\eta_n(\theta) = J_n^2(\theta), \qquad \theta = 4\pi g/\lambda, \tag{1}$$

where g is the grating amplitude. The 0 order corresponds to the planar state and is blocked. To achieve intensity modulation at the screen, power must be shifted to the other orders. A theoretical efficiency of 90% can be reached around $\theta = 0.6\pi$ for a configuration using the first and second orders. This phase-shift is translated into a total peak-to-valley deformation of 0.30λ, which is in the order of 150nm for visible light.

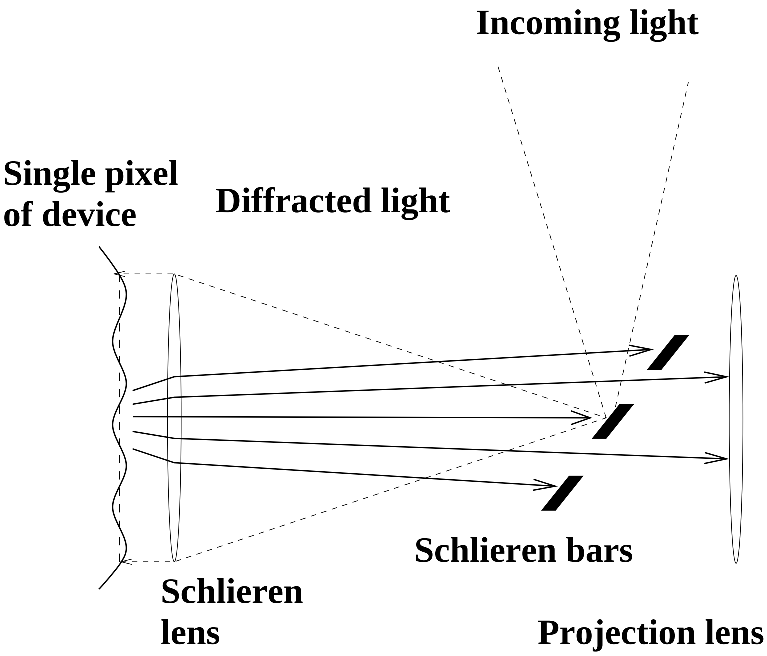

Figure 2. Operating principle for a single pixel in non-actuated state (dashed lines) and in actuated state (solid lines).

2.1.2. Two-dimensional modulators

Imaging systems require the use as 2D modulators. However, interest has also been shown in linear 1D electrically deformable gratings. The advantage of such a grating is that there is minimal scattering due do diffraction at sharp edges, since the surface is inherently smooth. Since such components are not yet widely available, it is possible that new applications will emerge, both in the area of actuators and sensors, e.g. in the field of spectrography.

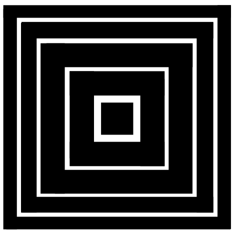

Figure 3. Example of an alternative electrode pattern.

2.1.3. Technology and results

The fabrication technology takes a novel approach to the previously existing idea of metallized viscoelastic surfaces. Instead of evaporating the metal layer on a spin-coated and planarized layer of viscoelastic material,[8,9] the layer is formed optimally on a static carrier chip, after which the viscoelastic layer is cured (and thus planarized) against this chip. Finally, removal of the carrier completes the thin-film transfer method.

This assembly is shown for a single pixel in Fig. 4: the carrier chip with the mechanical (metal) layers is placed over the active area of the driver chip. A droplet of the viscoelastic material is placed in between and the two are pressed together until the spacers are reached.

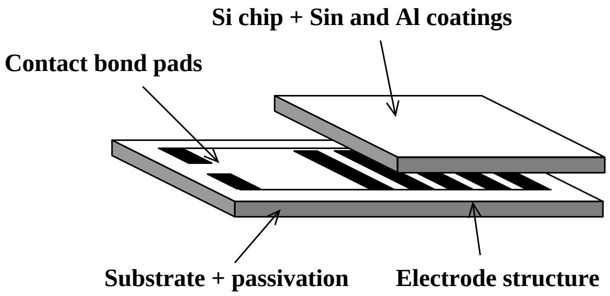

Figure 4. Schematic diagram of the experimental design prior to deposition of the elastic layer.

Two techniques used to remove the carrier chip are:

1. Bulk-etching steps to dissolve the carrier chip: a bulk silicon chip is coated with 50nm of SiN and 80nm of Al. After bonding, the top chip is etched in a KOH solution, stopping on the nitride film.
2. Lift-off for transfer of layers without etching steps or elevated temperatures: the metal layer is deposited on a thin sacrificial material or on a base with poor adhesion. Gold-coated modulators have been made by evaporating a 125nm Au layer on a silicon base without an intermediate Cr layer. After removing the carrier, the thin metal layer stays behind.

Photographs of mounted devices using either technique are shown in Fig. 5.

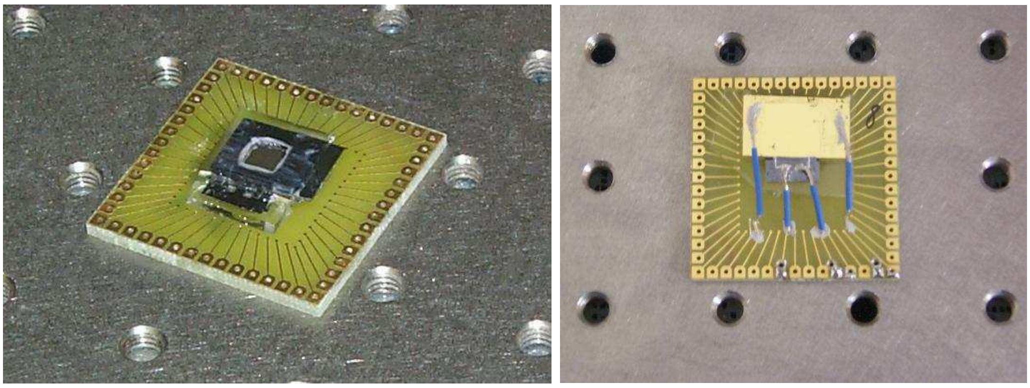

Figure 5. Photographs of mounted VSLMs for bulk-etching techniques (left) and lift-off techniques (right).

Modulators using lift-off techniques show most promising results and require the least complex combination of processing steps. When potentials are applied between the membrane and one of the contact pads, we obtain the far-field scattering pattern shown in Fig. 6. The centers of each order are each spaced at 7.2mm at a total distance of 2.47m, meaning a first-order angle of 2.91 mrad.

The static regions surrounding the active area cause the large bright spot in the picture and are the reason for the brightness in the zero order in spite of modulation.

Response times were measured by taking the intensity in the third order under the application of a input periodic pulse V_S. It is seen that the rise time is very fast (order of 1-5ms), while the return time is considerably longer, owing to elastic relaxation. Alternate driving (i.e. actively restoring planar state) is expected to shorten the return time.

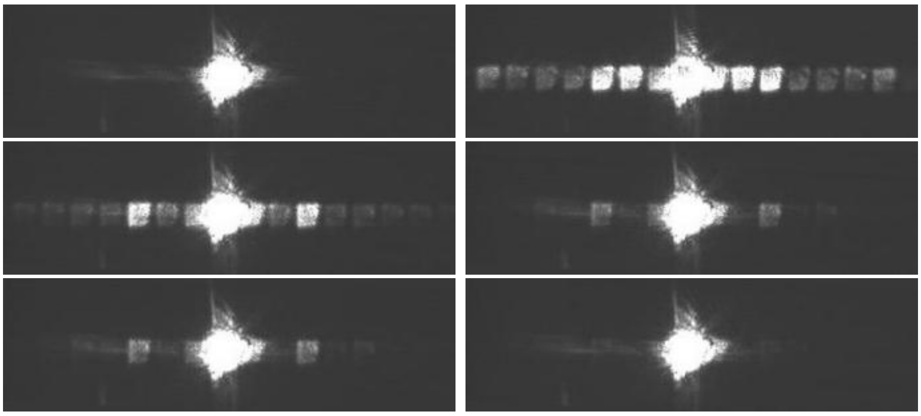

Figure 6. Far-field scattering pattern for increasing V_S up to 200V and back again to 0V.

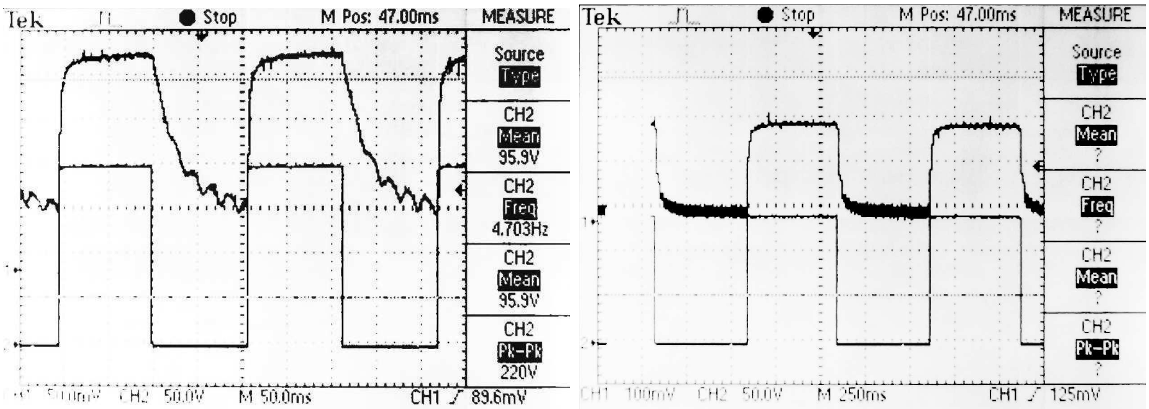

Figure 7. Graphs of response times to a rectangular signal pulse on V_S.

Optimized driving schemes (active return to planar state) can lead to gray-scale frame rates around 200Hz. For displays, this is very adequate, as higher frequencies are not required to simulate intermediate states by means of duty cycle modulation.

2.1.4. Technical benefits

Some of the expected benefits of this technology are itemized below:

- Experience with thin-film transfer techniques exists that is optimized both for quality and simplicity of fabrication.
- CMOS circuitry can be produced in bulk; needs to drive an array of gratings. Mechanical layers require only two main additional steps.
- It is expected that by using the correct driving scheme, viscoelastic layer material and further optimization of the transfer technique, very inexpensive and stable modulators can result.
- High demand already exists for inexpensive solid-state Eidophor alternatives.
- Generic and inexpensive nature of the technology will broaden range of practical use. Any context needing an electrically controllable phase grating becomes a potential application.

3. LIQUID-CRYSTAL MODAL WAVEFRONT CORRECTORS

Liquid crystals (LCs) are ubiquitous in display applications and their electro-optical characteristics are well understood.

Ferroelectric LCs are often used in applications where a high switching speed is required and binary modulation is enough (including displays). The majority of LC displays, however, is based on twist and super-twist effects in nematic LCs,[12, 13] which allow grayscale modulation. Nematic LCs are attractive for phase modulation, because of the controllability of their birefringence with an applied voltage; and the change of phase of a transmitted polarized light beam is directly proportional to the change of birefringence.

Despite the relatively slow LC response times (typically hundreds of ms), LC phase modulators represent a feasible and inexpensive alternative to deformable mirrors because of some particularly attractive characteristics: large amplitude of the controllable phase-delay (tens of wavelengths), low power consumption (0.1 mW/cm^2), absence of moving parts and low control voltages (compatible with CMOS technology).

3.1. Proposed approach

Several liquid-crystal (LC) correctors are available commercially. They are mostly based on a discrete structure of actuators and their operation resembles that of piston-type segmented mirrors, which prompt a step-wise approximation to wavefronts, i.e. to smooth continuous functions.

Often, a large number of actuators (more than one hundred) are required for satisfactory approximation of low-order aberrations. To overcome the previous demand, an LC corrector with modal response was proposed in order to provide a spatially continuous phase modulation and a reasonable approximation to low-order aberrations even for a small number (several tens) of actuators. It was shown that this device can operate with one or two control parameters (degrees of freedom) per actuator, depending on the requirements to the quality of the approximation.

3.2. Practical devices

The schematics of a reflective modal LC corrector is depicted in Fig. 8. An LC layer is positioned above a continuous highly resistive layer (sheet resistance $\sim$ 0.1-1MΩ/sq) with a grid of metal contacts, to which AC control voltages are applied. The resistive layer is covered with a reflective dielectric surface. The continuous voltage variation over the resistive layer ensures a smooth birefringence variation of the LC layer, therefore resulting in a smooth phase modulation over the optical aperture.

A particular feature that distinguishes modal LC wavefront correctors from other types of modal correctors is the possibility to drive each actuator with several degrees of freedom: amplitude, frequency and phase of the AC control voltage. Variation of each of these parameters is proven to alter either the LC electro-optic response, or the interaction with the response of neighboring contacts, or both. Two control approaches were found to be the most useful: 1) amplitude modulation (fixed frequency and phase) and 2) combined amplitude and phase modulation (fixed frequency). The first method allows the use of a linear control algorithm and provides a correction quality close to that of deformable mirrors. The second method is better suitable to the fine tuning of the results of the first method, where optimization of the phase shifts can yield up to 65% improvement, as predicted by simulations - see Fig. 9.

A glass-based technology was used to fabricate 37-actuator devices with 30- and 70-mm apertures, which serve as a demonstration of the modal operation principle. This technology allows to manufacture devices with quite large aperture, which is an important advantage. However, the high costs and the unlikely compatibility with serial production calls for an alternative technology. Silicon-based technology offers a reasonable choice, especially because it is widely available and enables the integration of the optical and the electric/electronic parts on a single chip. It, therefore, allows reducing the number of inputs of the chip relative to the number of actuators, which makes the technology easily scalable.

In the framework of silicon microfabrication technology we designed a grid of 39 concentric Al/Si point electrodes connected to metal pads at the periphery of the chip. One of the main technical difficulties is in manufacturing of the resistive layer with a sheet resistance in the range of $\sim$ 0.1-1MΩ/sq. Recently these

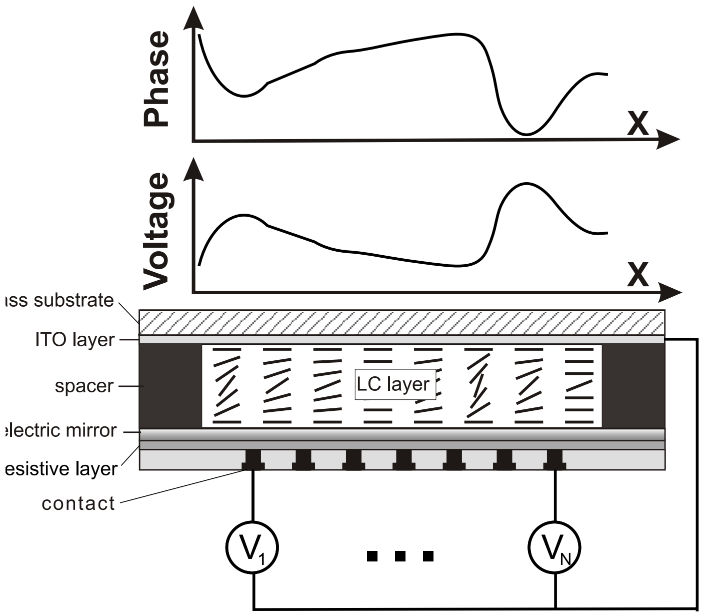

Figure 8. Schematics of an LC modal wavefront corrector.

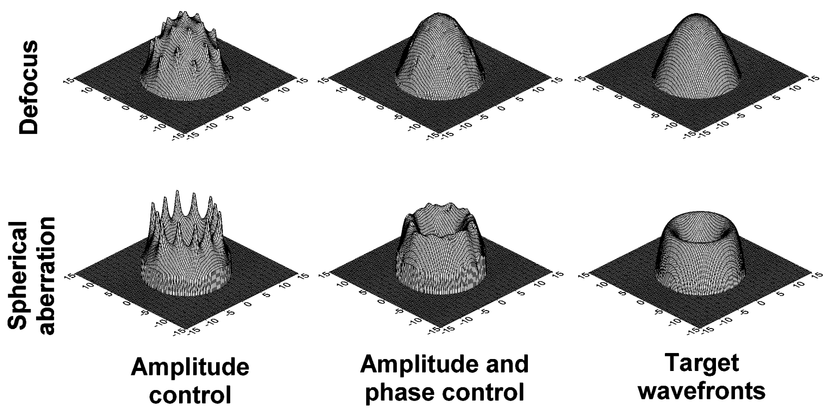

Figure 9. Examples of defocus and spherical aberration approximation in a LC modal wavefront corrector.

properties were demonstrated for thin films of n-type doped silicon carbide, which were deposited using PECVD (Plasma Enhanced Chemical Vapor Deposition) technology and then annealed with an excimer laser operating in the UV range. However, the issues of patterning of this layer and the layers above with no damage to its conductive properties are yet to be solved.

The feasibility of the proposed approach was demonstrated by results of both simulation of the modal LC corrector and experimental investigation of its prototype. Its practical implementation using silicon technology, however, can be done indirectly. In particular, it is possible to combine zonal and modal approaches by replacing a continuous resistive layer by a network of discrete IC resistors. A modulator with a large amount of pixels driven by a smaller number of control channels can be produced in this way. Our present investigations are also focused on this idea.

4. MICROMACHINED MEMBRANE DEFORMABLE MIRRORS (MMDM)

A Micromachined Membrane Deformable Mirror (MMDM)[14] consists of a thin stretched membrane suspended over an array of electrostatic electrodes as shown in Fig. 10. The membrane is fabricated by LPCVD deposition of a thin $\sim$0.5μm layer of tensile stressed silicon nitride Si_nN_m, followed by anisotropic etching of bulk silicon to release the membrane. Pure nitride membranes are sufficiently strong for mirrors with diameters of up to 25mm, larger membranes – up to 50mm – can be fabricated by sandwiching a relatively thick – up to 10μm – layer of epi-poly silicon between two nitride layers.

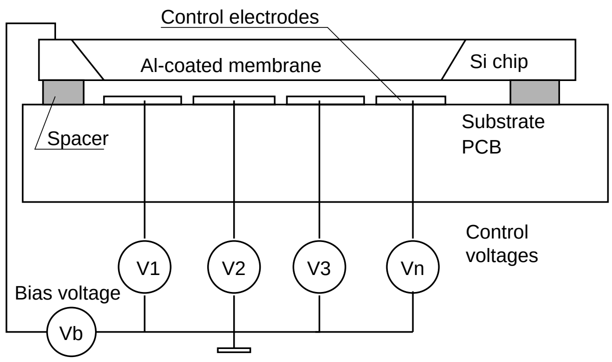

Figure 10. Schematic section of the micromachined adaptive mirror.

In the simplest case the membrane is coated by a thin layer of metal – aluminum or gold – providing sufficiently reflective broadband coatings in the visible (Al) and infrared (gold) regions. In case a higher reflectivity is required (for instance for laser intracavity applications), the membrane can be coated with Cr/Ag composition followed by up to 12 dielectric layers, resulting in reflectivity of up to 99.8% in a narrow spectral region. Multilayer coated mirrors reported to work with laser loads of up to 550W in a 5mm circular beam at λ=1.06μm.

The initially flat membrane can be deformed only towards the electrostatic actuators because the electrostatic force can be only attractive. This limits the possible optical figures of the MMDM to be always concave. Since most of the applications require both convex and concave operation of the mirror, the initial mirror figure is electrically biased to take a concave parabolic shape, median with respect to zero and maximum deflection. From this position, the mirror can correct both concave and convex aberrations with relation to the parabolically biased figure. The typical response time is $\sim$1ms, making the mirror suitable for real-time control of turbulence-induced aberrations.

Since the technology of MMDM is based completely on inorganic materials, devices were demonstrated to work in vacuum at cryogenic temperatures down to T=78K,[15] which makes them potentially suitable for space-based adaptive optics.

MMDM is reported to be successfully used for real-time correction of phase aberrations in laboratory and in a one meter telescope at Apache Point, New Mexico .[16] In particular, the Strehl ratio was improved in average from 0.08 to 0.48 for simulated turbulence in the laboratory, and from 0.04 to 0.1 in a 10-exposure field experiment with Altair image.

Small size, quick response, high density of actuators, smooth modal response and hysteresis-free operation make MMDM highly suitable for feed-forward correction using control approach based on a combination of optimization with program control. In the beginning, the voltage vector applied to the mirror electrodes is optimized to obtain the maximum of the the appropriate quality parameter – brightness for laser systems, sharpness and image quality for imaging systems, pulse duration for ultrafast lasers. The optimization process can take up to several thousand iterations and usually results in significant improvement of the quality of the optical system. The control vector is written in the memory of the computer and can be recalled every time the control situation repeats.

Based on this approach, a wide field correction of scanning optical microscope was demonstrated in.[17] The scanning beam quality was individually optimized for each point in the field of view and the lookup table of MMDM control vectors was stored in the computer. In the operation mode, the scanning beam was corrected "on the fly" for each scan position, resulting in drastic improvement of the microscope resolution over the whole field.

Another example of the optimization approach combined with a lookup table is given in[18] – where the authors report on a 1xN optical switch with MMDM used to improve coupling efficiency in each switch channel of a fiber switch by pre-setting the mirror shape in accordance with the lookup table.

Optimization approach proved very efficient in numerous experiments with compression and optimization of ultrafast optical pulses. A special MMDM was developed for one-dimensional correction of phase aberrations along a single line. These devices are usually used in a stretcher of ultrafast laser to balance phase delays of spectral components. Optimization of the spectral phase resulted in efficient compression of femtosecond pulses and even in improvement of the efficiency of a EUV plasma source.[19–21]

MMDMs were also successfully used for wavefront correction in terawatt lasers[22] and for intracavity control of high-power industrial lasers.[23, 24]

Finally, MMDM are suitable for real-time correction of the aberrations of the human eye, making possible "electronic spectacles" for real-time improvement of the vision acuity.[25]

Compactness, simplicity and high optical quality make MMDM the device of choice for a number of optical applications in the laser optics, imaging, optical testing and astronomy.

5. WAVEFRONT SENSORS COMPATIBLE WITH CMOS TECHNOLOGY

5.1. The Hartmann-Shack method

A wavefront sensor can be used both to assess the quality of a wavefront and to effectively drive an adaptive corrector. The most widely used wavefront-sensing technique in adaptive optics is the Hartmann-Shack method, in which a microlens array samples a wavefront into patches (Fig. 11). The average wavefront tilt of each patch results in a displacement of the corresponding focal spot, with respect to a reference position, on the focal plane. Therefore, the wavefront shape can be estimated based on spot displacements. In the case of mirror control, a feedback loop attempts to ensure an optimal mirror shape, based on the sensor output, for which the spot centroids coincide with the reference positions, i.e., the mirror attempts to recreate the reference wavefront from an incoming distorted wavefront.

5.2. Conventional approach

Conventional Hartmann-Shack wavefront sensors employ a camera (e.g. CCD or CMOS)for the detection of the light spots. This becomes an issue when high-speed operation is required: the frame rate of off-the-shelf cameras is limited (usually not larger than 150fps) and the resulting frame needs to be processed in order to yield the spot displacements. Fast cameras do exist but are usually very expensive (a 4kHz CMOS camera costs today around 100K USD) and there is no direct link between high speed and good resolution, or high quantum efficiency, or low noise. Moreover, the bitmap resulting from these cameras still need to be processed. Some CMOS cameras feature framing (windowing) in which a sub-frame can be specified and readout faster than the global image.

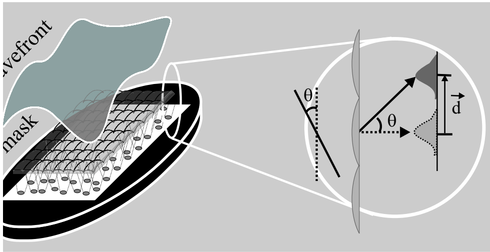

Figure 11. The Hartmann-Shack principle.

The remaining issue is whether the sub-frame contains enough pixels to allow the accurate detection of a number of light spots (typically from 25 to 1000). The lateral size of the sub-frame should also be able to accommodate all the spots whereas preventing overlap between them (the pitch of the spot grid varies from 200μm to 1500μm. There are also CMOS cameras with a multiple-framing feature, in which case, each spot could be associated with a frame resulting in faster processing (irrelevant 'dark' pixels are not read out), however, frame switching takes considerably long and the global output is possible not significantly advantageous.

5.3. Custom approach

The use of a matrix of position-sensitive detectors (PSDs) offers an alternative to a conventional camera in order to obtain faster operational frequencies. Each PSD is associated with a sampled light spot, resulting in nearly direct information about the positions of the spots. This approach has two main advantages: it does not contain dummy pixels (those not effectively used in the determination of the spot position)and it substitutes the image-processing step with a simple calculation based on the PSD output signals. A sketch contrasting these two approaches is shown in Fig. 12.

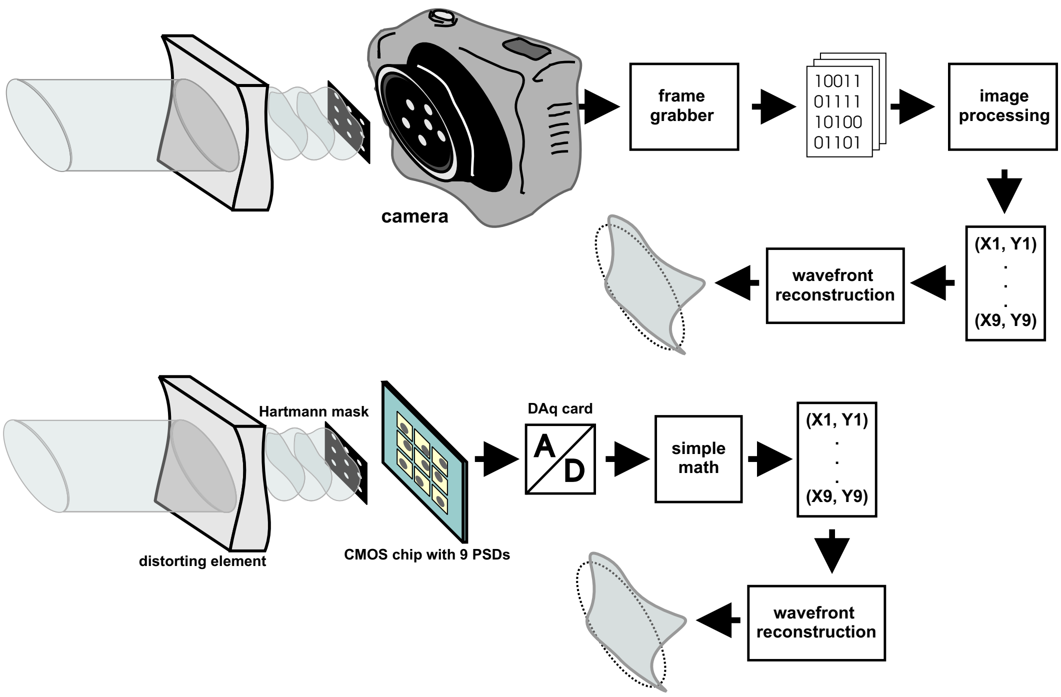

Figure 12. Sketch illustrating the approaches using a conventional camera and a custom chip with position-sensitive detectors.

Among several standard technologies available for the fabrication of this custom chip, CMOS (Complementary Metal-Oxide-Semiconductor technology) represents a sensible choice, not only because the process is largely available and a wafer run is cost effective but, more importantly, because CMOS is receptive to custom architectures and electronic functions. It accommodates both digital and analog circuitry on a single chip and enables the implementation of a number os photosensitive structures. The steady market interest in this technology promotes expanding circuit solutions and reliable modelling of devices.

5.4. Fabricated CMOS wavefront sensors

To date, three different versions of PSD-based wavefront sensors have been fabricated in standard CMOS:

1. Delft1: 1.6μm - DIMES - 8x8PSDs quad cell - passive pixels.[26,27]

   This sensor was designed at Delft University of Technology (The Netherlands). The chip is 10mmx10mm and was fabricated in a 1.6μm CMOS process. It comprises 64 quad cells arranged in a orthogonal array and a analog demultiplexer that enables random access to the pixels. Each quad cell consists of four pixels, each with a 300μmx300μm photodiode and a switch set. The normalized response of the quad cell to a spot movement in the x direction is only linear in its very center, but can be closely approximated over the whole displacement range by the following relation:

   $$x_{PSD} = A_2 + \frac{(A_1 - A_2)}{(1 + exp(x/s_x))} \quad , \tag{2}$$

   where A_1, A_2 and s_x are the minimum x value, the maximum x value and the slope parameter, respectively.[28] These quantities depend on the spot profile and on the ratio of the effective radius to the quad-cell lateral size. If the spot is symmetrical, then the y response can be approximated by the same equation.

   This wavefront sensor requires light spots with intensities on the order of μW, but it is able to operate at 3kHz and features a very good position resolution (1μm) and therefore a good wavefront accuracy, on the order of $\lambda/50$ ($\lambda = 633nm$) @ $10\mu W$/spot.

2. Heidelberg1: 0.6μm - AMS - 16x16PSDs alternate - winner-take-all - digital readout.[29]

   This sensor was designed at the University of Heidelberg (Germany) and features 16x16 alternate-structure PSDs. The chip size is 7.7mmx8.2mm. Each PSD consists of 19x19 pixels and two independent readout winner-take-all (WTA)chains for the detection of the x and the y positions, respectively. Each pixel line, or column, is connected to a node of the corresponding WTA chain. The input node with the largest photocurrent yields a digital 'one' at the respective output node; all other output nodes yield a digital 'zero': $x_{PSD} = [..., 0, 0, 1, 0, ...]$.

   This approach detects the spot centroid position based on the spot peak intensity. This limits the position resolution to the pixel pitch (17.6μm) of the PSD, but allows operation at very low light levels, on the order on nW.

3. Heidelberg2: 0.35μm - AMS, 8x8PSDs chessboard-like - winner-take-all - resistive ring.[30]

   This chip measures 4.1mmx4.1mm and contains 8x8PSDs, each of which is implemented with 21x21 pixels arranged in a chessboard-like structure. It uses multiple WTA sub-chains connected via a resistive ring, which yields a response of the type $x_{PSD} = [..., 0, 0, 1, 1, 1, 0, ...]$. This is used for pseudo-centroiding estimation of the spot position, i.e., the spot centroid is calculated based on the average of several peak intensities. This chip is able to operate at 4kHz and with tens of pW per spot but the position resolution is still limited by the pixel size (17μm).

The sensors Delft1 and Heidelberg2 still have plenty of room for improvement, while still keeping their current advantages. The first will be able to operate at much lower light levels if active pixels are used and lower-junction photodiodes are chosen, reducing the dominating capacitive noise. The latter can improve the spot-position resolution by using appropriate temporal post processing of the signal on chip. Furthermore, both chips, in principle, can profit from a hardware-based neural network for wavefront reconstruction on chip, eliminating the computer as the processor unit.

6. MICROMIRROR AND MICROLENS ARRAYS

To sample a wavefront in the Hartmann sensor we can use either a microlens array or a Hartmann mask, which is simply an opaque mask with a grid of openings. Both can be fabricated cost effectively in the framework of single-mask etching technologies.

We make high-precision Hartmann masks by depositing an Aluminum layer on a glass substrate and then by using reactive ion etching to create the openings in the metal layer. The opening geometry and the grid grid pitch are defined with lithographic precision ($\leq 1\mu$m).

The substitution of a Hartmann mask with a microlens array has several advantages: higher light-collection efficiency, less sampling alias and insensitivity to intensity variations over the sub-aperture. Some of the most desired characteristics of these arrays for a Hartmann-Shack sensor are: parallelism of the optical axes, position precision and 100% fill factor. However, methods for the fabrication of microlens arrays are usually costly, or complex, or both.

We used a novel and inexpensive method for the fabrication of micromirror arrays in silicon, from which the microlens arrays are replicated. The method requires a single mask with a grid of openings and consists of two etch steps in a KOH solution: 1) etching of silicon through an oxide mask to achieve pyramidal pits, 2) etching of the pyramidal pits, after the removal of the mask, to achieve spherical cavities.[31, 32] Fig. 13 shows the results of these two steps. The sagittae of the cavities and their diameters depend on the size of the initial opening; the diameters also depend on the etch depth.

We can choose an arbitrary array geometry, e.g. hexagonal and orthogonal grids that yield identical microlenses with no gap between them. The lateral overlap of the spherical cavities ensures 100% fill factor and a very sharp interface. The paralellism of the optical axes is determined by the crystal orientation and is therefore very high; and the position of the microlenses is determined by the lithographic precision ($\leq 1\mu$m); the cavity profile is highly spherical ($\leq 10nm$ deviation). The microlens array is replicated by pressing a polymer against the micromirror template. The resulting rms surface roughness lies around 20nm, which can be translated as a Strehl ratio larger than 0.98 ($\lambda = 633nm$).

The focal length depends on the initial opening dimension d_0, on the etch depth h and on the refraction index n of the material used for the replication, as indicated in Eq. 3.

$$f = 7.6\frac{d_0}{\alpha(n-1)}(\frac{h}{d_0})^{0.58} \quad , \tag{3}$$

We present in Fig. 14 an hexagonal micromirror array with 127 elements and 300μm grid pitch, from which we replicated a close-packed array of microlenses with 17mm focal length and 85μm spot diameter.

7. MICRO-OPTICAL COMPONENTS WITH ARBITRARY ASPHERICAL SHAPES

There is a diversity of applications in which aspherical micro-optical elements can be used, e.g. optical telecommunications, beam forming optics, hybrid wavefront sensors, beam shaping and displays. We developed a method, based on the technology presented in the previous section, in which we approximate arbitrary surfaces by overlaying NxN spherical cavities with different sagittae and diameters.[33] The sagitta s of each cavity is proportional to the size of the respective initial opening d_0 on the oxide mask: $s = \alpha d_0$, where α is a parameter that depends on the etch ratio between different planes, on the etchant concentration and on the etching temperature.

The accuracy of the approximation depends on two uncorrelated parameters: the structural roughness and the intrinsic roughness. The structural roughness is related to the pit density, the pit sizes and the etch depth, whereas the intrinsic roughness relates to the etchant parameters and to the etch depth.

This technique enables the fabrication of aspherical templates, from which refractive phase plates are replicated. We fabricated a number of phase plates reproducing Zernike polynomials: tilt, defocus, astigmatism, spherical aberration and higher order terms, with 1mm and 5mm lateral sizes and with ~ 1650 and $400\ pits/mm^2$, respectively. Fig. 15 shows the interferometric patterns corresponding to replicated astigmatic lenses. The 5mm astigmatic lens has a maximum amplitude of 8μm, whereas the 1mm lens has an amplitude of 3μm. Fig. 15 also

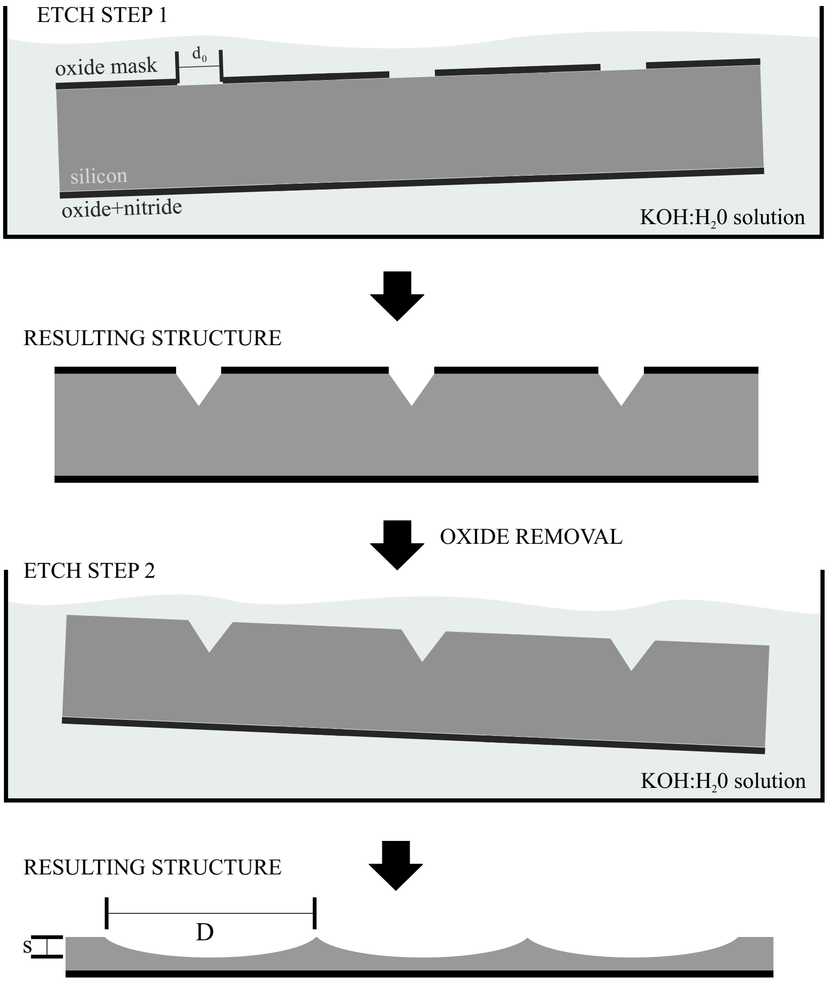

Figure 13. Simple two-step bulk silicon etching results in smooth spherical cavities.

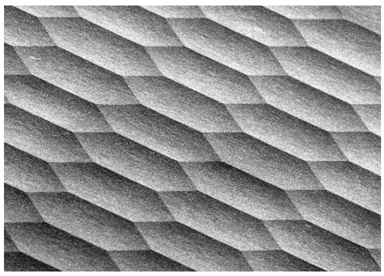

Figure 14. SEM picture of a fabricated hexagonal micromirror array with 100% fill factor.

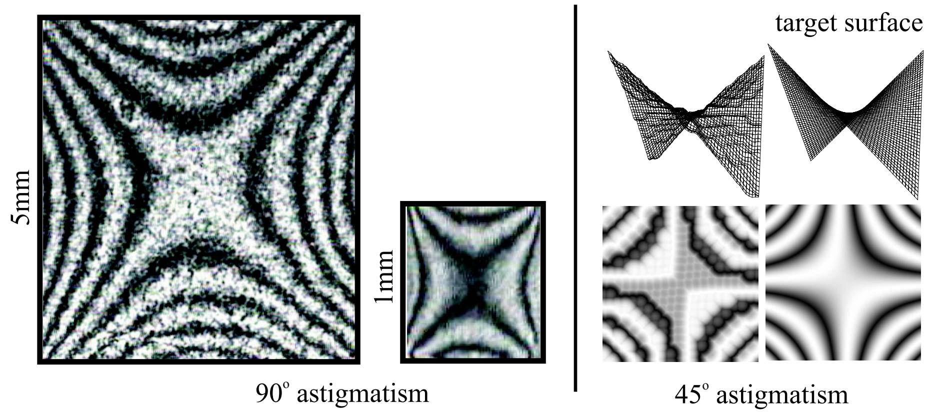

Figure 15. Left: interferometric pattern of replicated astigmatic phase plates: 5mmx5mm structure (8μm amplitude)approximated with 1650 $pits/mm^2$, 1mmx1mm structure (3μm amplitude) approximated with 400 $pits/mm^2$. Right: interferometric pattern of a simulated approximation to a $1mm^2$ 45^o astigmatic mirror with 400 $pits/mm^2$.

shows the simulated approximation of a 1mm 45^o astigmatic structure with only 400 $pits/mm^2$, which enables us to more clearly visualize the role of pit density in the surface quality.

The simple and inexpensive technology presented here is suitable for serial production of high-quality reflective and refractive micro-optical components with an arbitrary shape.

8. CONCLUSIONS

We successfully fabricated several micro-optical devices and components for wavefront detection and control in the framework of silicon microtechnologies. The reported fabrication approaches offer substantial benefits over traditional approaches, especially the possibility to combine low-cost manufacturing with functionality and system integration.

ACKNOWLEDGMENTS

MOSIS funded part of the research on MMDMS (ESPRIT-31063), and The Dutch Technical Foundation (STW) funded projects on SLMs (DEL.55.3945), on LC correctors (DOE.5490) and on the CMOS wavefront sensor (DOE.5375).

REFERENCES

1. H.L. Ong, "Microdisplay Opportunity: Small Size, Low Power, Big Image, Bright Future", Proc. SPIE,Vol. 3560, p. 1-12, 1998.
2. S. Dash, "Market Trends in the Projection Display Industry", Proc. SPIE, Vol. 4294, p. 1-12, 2001.
3. H.L. Ong, "Microdisplay Opportunity: Small Size, Low Power, Big Image, Bright Future", Proc. SPIE, Vol. 3560, p. 1-12, 1998.
4. K.E. Petersen, "Silicon as a Mechanical Material", Proc. IEEE, Vol. 70, no. 5, p. 420-457, 1982.
5. J.B. Bryzek, K. Petersen and W. McCulley, "Micromachines on the march", IEEE Spectruym, VOl. 31, no. 5, p. 20-31, 1994.
6. E. Labin, "The Eidophor method for theater television", SMTPE Journal, 54, p. 393-406, 1950.
7. S.A. Williams, "History of Eidophor Projection in North America", Proc. SPIE, Vol. 3013, p. 7-13, 1997.
8. H. Kück, et al, "Deformable micromirror devices as phase-modulating high-resolution light valves", Sensors and Actuators A 54, 1996, p. 536-541.
9. W. Brinker, et al, "Metallized viscoelastic control layers", Displays 16, no. 1, p.14-20, 1995.
10. C.W. McLaughlin, D. Armitage, "Prospects for microdisplay based rear projection", Proc. SPIE, Vol. 3296, p. 2-12, 1998.

11. W.E. Glenn, "The Development of Electronic Cinema Projectors", Proc. SPIE, Vol. 4294, p. 13-20, 2001.
12. P.J.Collins, J.S.Patel (eds.), Handbook of Liquid Crystal Research, Oxford University Press, 1997.
13. V.G.Chigrinov, Liquid Crystal Devices: Physics and Apllications, Artech House, Boston, 1999.
14. G. Vdovin, S. Middelhoek, P.M. Sarro, "Technology and applications of micromachined silicon adaptive mirrors", Optical Engineering **36**, p. 1382-1390, (1997)
15. H.M. Dyson, R.M. Sharples, N.A. Dipper, G.V. Vdovin, Optics Express, **8/1**, (Jan 2001)
16. D. Dayton, S. Restaino, J. Gonglewski, J. Gallegos, S. McDermott, S. Browne, S. Rogers, M. Vaidyanathan, M. Shilko, Optics Communications, **176**, 339-345 (2000)
17. O. Albert, L. Sherman, G. Mourou, T.B. Norris, G. Vdovin, Optics Letters **25/1**, 52-54 (2000)
18. F. Gonte, A. Courteville, R. Dandliker, Optical Engineering **41 (5)**, 1073-1076 (2002)
19. E. Zeek, R. Bartels, M.M. Murnane, H.C. Kapteyn, S. Backus, G. Vdovin, Optics Letters, **25/8**, 587-589, (2000)
20. A. Baltuska, T. Fuji, T. Kobayashi, Optics Letters, **27/5**, 306-308, (2002)
21. R. Bartels, S. Backus, E. Zeek, L. Misoguti, G. Vdovin, I.P. Christov, M.M. Murnane, H.C. Kapteyn, Nature, **406**, 164, (Jul 2000)
22. F. Druon, G. Cheraux, J. Faure, J. Nees, M. Nantel, A. Maksimchuk, G. Mourou, J.C. Chanteloup, G. Vdovin, Optics Letters **23** 1043 (1998)
23. G. Vdovin, V. Kiyko, Optics Letters **26/11**, 798-800 (2001)
24. W. Lubeigt, G. Valentine, J. Girkin, E. Bente, D. Burns, Optics Express **10/13**, 550-555 (2002)
25. E. Fernandez, I. Iglesias, P. Artal, Optics Letters, **26/10** 746-748, (2001)
26. D. W. de Lima Monteiro, G. Vdovin and P. Sarro, "High-speed wavefront sensor compatible with standard CMOS technology," To be published in Sensors and Acutators A, (expected: February 2004)
27. D. W. de Lima Monteiro, G. Vdovin et al., " Customized CMOS wavefront sensor," Proc. SPIE **4493**, 88-99 (August 2001)
28. D. W. de Lima Monteiro, "CMOS-based integrated wavefront sensor," Delft University Press, Delft, (2002)
29. D. Droste and J. Bille, "An ASIC for Hartmann-Shack wavefront detection," IEEE Journal of Solid State Circuits, **37**, 173-182 (2002)
30. T. Nirmaier, G. Pudasaini and J. Bille, "Very fast wave-front measurements at the human eye with a custom CMOS-based Hartmann-Shack sensor," Opt. Express 11, 2704-2716 (2003)
31. D. W. de Lima Monteiro, O. Akhzar-Mehr and G. Vdovin, "Prime microlens arrays for Hartmann-Shack sensors - An economical fabrication technology," To be published in the Proc. AO Workshop for Industry and Medicine , Muenster-Germany (Oct.2003), (expected: March 2004)
32. D. Kendal et al, Opt. Eng. **33** (11), 3578-3588, (1994)
33. D. W. de Lima Monteiro, O. Akhzar-Mehr, P. M. Sarro and G. Vdovin, "Single-mask microfabrication technology of aspherical optics using KOH anisotropic etching," Opt. Express 11 (18), 2244-2252 (2003)